

Bonding of Zr₄₄Ti₁₁Cu₁₀Ni₁₀Be₂₅ bulk metallic glass and AZ31B magnesium alloy by hot staking extrusion

Weilu Zhou, Huiping Li*, Zhichao Li, Xibin Zhu, Lianfang He

School of Materials Science and Engineering, Shandong University of Science and Technology, Qingdao, Shandong, 266590, China

ARTICLE INFO

Keywords:
Bulk metallic glass
Stacking extrusion
Bonding
Interface

ABSTRACT

A new Zr₄₄Ti₁₁Cu₁₀Ni₁₀Be₂₅ (LM1B) bulk metallic glass (BMG) and AZ31B Mg alloy composites were prepared by hot stacking extrusion process based on the thermoplastic forming ability of LM1B BMG within the supercooled liquid range (SLR). The stacking extrusion tests were carried out at three different temperature of 430 °C, 440 °C and 450 °C, respectively, and the extrusion speed was 5 mm/min. Morphology and structure of the extruded samples were characterized by the different methods. The results indicated that the LM1B BMG and AZ31B magnesium alloy can be well bonded, and welding defects at the smooth and continuous interface were negligible. The bonding mode is mainly mechanical bonding, meanwhile, a few of metallurgical bonding does exists. Significant atomic diffusion was detected in the vicinity of the interface, while the nanocrystals and partial crystallization were produced in the LM1B BMG.

1. Introduction

Bulk metallic glasses (BMGs) have excellent physical, chemical and mechanical properties at room temperature, such as high strength and hardness, perfect wear resistance and corrosion resistance [1,2]. As structural materials, BMGs have a promising potential for engineering application. It can replace the existing high-performance metals to manufacture the key working parts of equipment, and it is one kind of engineering materials having a wide application prospect. Recently, with the development of the preparation technology of BMGs, the cooling rate required for the preparation of BMGs is obviously reduced, and the thickness of BMGs can reach 25 mm [3], which greatly broadens the range of parts that can be manufactured by BMGs.

At a temperature far below the glass transition temperature (Tg) and with a high strain rate, BMGs usually exhibit inhomogeneous deformation controlled by a single shear band propagation mechanism. Moreover, the deformation of BMGs shows a high degree of localization at room temperature. That is the deformation is concentrated in a few narrow shear bands, which easily leads to catastrophic fracture of BMGs without macroscopic plastic deformation [2,4]. When plastic deformation is carried out at the certain strain rate in the supercooled liquid range (SLR), BMGs presents a viscous fluid state and uniform deformation, and exhibits excellent superplasticity under the action of

external force [5,6]. At present, the size, forming ability and weldability of BMGs are some of the most important factors restricting the engineering application of BMGs. And it is very significant for engineering application of BMGs to study the its plastic forming and welding processes in the SLR.

For engineering application of BMGs, it is necessary to establish the metallurgical bonding technology. It has been reported that BMGs were successfully welded together by brazing [7,8], friction welding [9–11], electric beam welding [12,13], laser welding [14,15] and so on. Moreover, BMGs have been welded with crystalline material by friction welding [11] and electric beam welding [12]. The electric beam welding and laser welding belong to liquid phase welding. The electron beam welding technique requires harsh vacuum and high surface smoothness. In addition, the electron beam and laser welding techniques can easily lead to crystallization of BMGs and other inevitable defects, such as holes and cracks, while these defects often occur in the welding process between metals. Friction welding is one type of super cooled liquid phase welding. The main challenges for the friction stir welding are the complex technological parameters, ineluctable exit hole and the abrasion of stir pin [16]. The difficulty in combining BMGs with crystalline materials has become a key factor restricting the engineering application of BMGs. Moreover, many researchers were going to put more focus on the joining between BMGs and the crystalline material,

* Corresponding author. School of Materials Science and Engineering, Shandong University of Science and Technology, 579 Qianwangang Road, Qingdao, Shandong, 266510, PR China.

E-mail addresses: bylf201314@163.com (W. Zhou), lihuiping99@163.com (H. Li), lizc@sdu.edu.cn (Z. Li), 15266214920@163.com (X. Zhu), lf_he2007@126.com (L. He).

such as Ti, Cu, Al and so on.

Extrusion is one of the most important plastic forming process, it can be used to form the parts with a fixed cross-sectional profile and join the same type of materials [17] or two different types of materials [18–22] in the forming of materials. Lee et al. [18,19] demonstrated the bimetallic rods composed of Zr₄₄Ti₁₁Cu_{9.8}Ni_{10.2}Be₂₅ (LM1B) BMG and crystalline copper or LM1B BMG and crystalline aluminum alloys can be well fabricated by co-extrusion, the co-extrusion tests were carried out at the different temperatures and punch speeds in the SLR of the LM1B BMG. Liu et al. [20] fabricated a BMG/Cu composite rod and a plate with a Cu₄₀Zr₄₄Ag₈Al₈ BMG core and a pure copper sleeve by the co-extrusion process. Good interface adhesion with metallurgical bonding was formed, corresponding to two diffusion layers of about 100 nm near the Cu and BMG parts. In the research of Gravier et al. [21], a BMG/Alloy rod with Zr_{41.2}Ti_{13.8}Cu_{12.5}Ni_{10.0}Be_{22.5} BMG in the core and aluminum alloy in a sleeve has been successfully elaborated by co-extrusion. SEM observations of the cross-section of the rod show that the interface between the glass and the alloy is defect-free. Jiang et al. [22] studied the joining between LM1B and 7075 Al alloy by the staking extrusion process, which was carried out at 440 °C and the ram speed of 2 mm/min. The results show that the cross-section between the LM1B and 7075 Al alloy is the intermetallic compound layer without crack in the vicinity of the interface.

BMGs display a low viscosity above the temperature T_g for a long time before crystallization at a certain temperature range, which provides an opportunity for thermoplastic forming. The objective of study is to research the feasibility of preparing BMG/light alloys composites involving LM1B BMG and magnesium alloys by stacking extrusion in the SLR, and the interface properties between LM1B BMG and magnesium alloys are also presented.

2. Experimental procedure

The amorphous rod of Zr₄₄Ti₁₁Cu_{9.8}Ni_{10.2}Be₂₅, also known as LM1B, was supplied by MATERION INC in the form of 10 mm diameter and 100 mm length. The states of LM1B BMG before extrusion were confirmed by the D/Max 2500 PC X-ray diffraction (XRD) as shown in Fig. 1 (a). The glass transition temperature T_g, crystallization temperature T_x and supercooled liquid phase region ($\Delta T = T_x - T_g$) of the LM1B BMG rod measured by differential scanning calorimetry (DSC) in argon atmosphere are approximately 356 °C, 462 °C and 106 °C, respectively, as shown in Fig. 1 (b). Some flat circular plates with the diameter of 10 mm and height of 2 mm were cut from LM1B BMG rod. Some cylinders with the diameter of 10 mm and height of 10 mm were cut from AZ31B magnesium alloy rod (Mg–3Al–1Zn, wt.%). The melting point of AZ31B is approximately 650 °C. The end surfaces of LM1B BMG plates and AZ31B magnesium alloy cylinders were polished and cleaned by an ultrasonic cleaner.

The dimension of die and position of LM1B plate and AZ31B cylinder are shown in Fig. 2. The materials of extrusion die and punch are

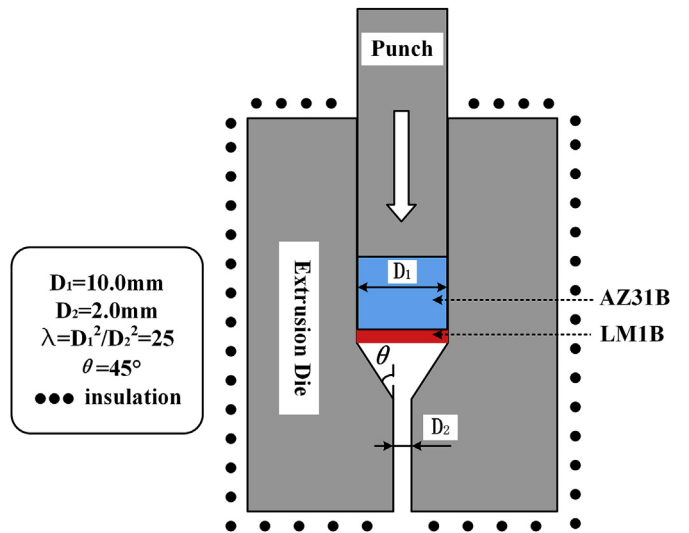


Fig. 2. Schematics of laboratory-scale staking extrusion apparatus.

H13 steel, the die is cut into two parts along the vertical direction to easily take out the part after extrusion. In the experiment, the die and punch are heated up to the setting temperature by four electrical bars inserted in the die, and the temperature is regulated by a KZ810 temperature controller. Graphite is chosen as a solid lubricant to decrease the friction coefficient between samples and the die. The die is surrounded by the aluminum silicate ceramic fiber paper to reduce the heat transfer between the die and environment in the extrusion process.

In the experiment, the punch speed is 5 mm/min, the heating temperature is 430 °C, 440 °C and 450 °C, respectively, as shown in Table 1. The experimental procedures are as following: (1) In order to minimize the heating time of LM1B BMG plate in the die, the die and punch are preheated to the setting temperature and keep the temperature for approximately 30 min to ensure the temperature uniformity of die and punch. (2) Take out the punch from the die, and then insert the LM1B BMG plate, Mg alloy cylinder and the punch in order. (3) Keep the setting temperature for approximately 2 min to ensure the temperature of LM1B BMG plate and Mg alloy cylinder reaching a same value as that of die and punch. (4) The LM1B BMG plate and Mg alloy cylinder are extruded at the punch speed is 5 mm/min by a WDW-200E servo-controlled electronic universal testing machine.

In order to investigate the macroscopic and microscopic characteristics of the extruded samples, the samples were cut into several parts around 15 mm in length. The morphology and microstructure in the vicinity of interface was observed by the Axiom LabA1 optical microscope (OM), Nova M450 scanning electron microscope (SEM) and FEI F200XG2 transmission electron microscope (TEM), respectively. The element distribution near the interface was obtained by means of FEI F200XG2 TEM. The LM1B BMG samples after extrusion were tested by

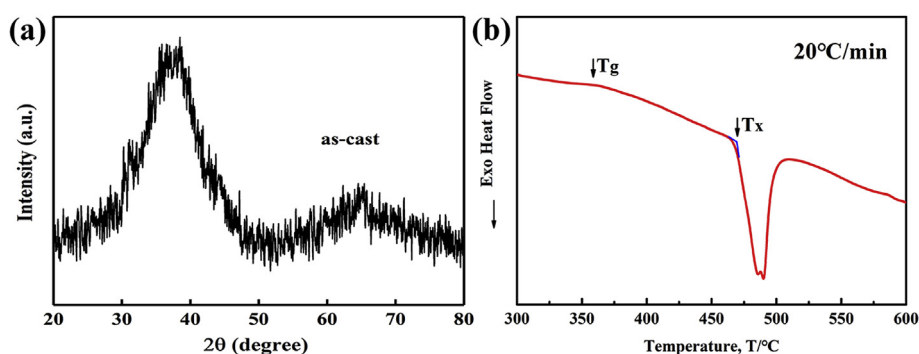


Fig. 1. XRD diffraction patterns and DSC curve of LM1B BMG, (a) XRD diffraction patterns of LM1B before extrusion, (b) DSC curve of LM1B.

Table 1
Staking extrusion test conditions.

Number	Temperature (°C)	Speed (mm/min)
1	430	5
2	440	5
3	450	5

the D/Max 2500 PC XRD.

3. Results and discussion

3.1. Staking extrusion behavior

Fig. 3 shows the appearance of samples before and after extrusion. As shown in Figs. 2 and 3 (a), the AZ31B sample is located above the LM1B sample before extrusion. Fig. 3(b–d) are samples attained in the experiment. There are three parts in the samples after extrusion, one is the full LM1B BMG, the other is the composite composed of AZ31B and LM1B, another is the full AZ31B, as seen in Fig. 3 (b). The split-type die has been employed in the test. The LM1B BMG will overflow along the parting surface of die and flash produces on the LM1B parts in the extrusion process, but there is not flash on the AZ31B part due to the better flow-ability of LM1B than that of AZ31B [22], as shown in Fig. 3 (c). It should be mentioned that high extrusion ratio with a small diameter outlet of die can result in a severe accumulating and blocking of materials in the cavity of die, which can easily cause the bending deformation of the initial extruded part due to the uniform extruding speed and friction coefficient on the surface of die outlet, as shown in Fig. 3 (d).

Fig. 4 presents the force-stroke curves in the extrusion of LM1B and AZ31B samples at the punch speed of 5 mm/min and the temperatures of 430 °C, 440 °C, 450 °C. There are five stages in the curves. For the sample extruded at 430 °C, the first is stage S1 on which the LM1B and AZ31B samples fill the cone-shape cavity of die at a rather slow rate, and the strain rate of materials is almost steady. The deformation behavior of BMGs significantly depends on the strain rate at the temperature within SLR [23], so the force is increased slightly, and the temperatures (430 °C, 440 °C, 450 °C) have no significant effect on the force. The second is stage S2 on which the deformation of LM1B and AZ31B samples can be called as upsetting, the gap (approximately 0.5 mm) between the die cavity and the cylindrical surface of samples will be filled up. The third is stage S3 on which the LM1B sample is firstly extruded into the outlet with the diameter of 2 mm, the force is increased due to the increasing of strain rate of LM1B sample close to

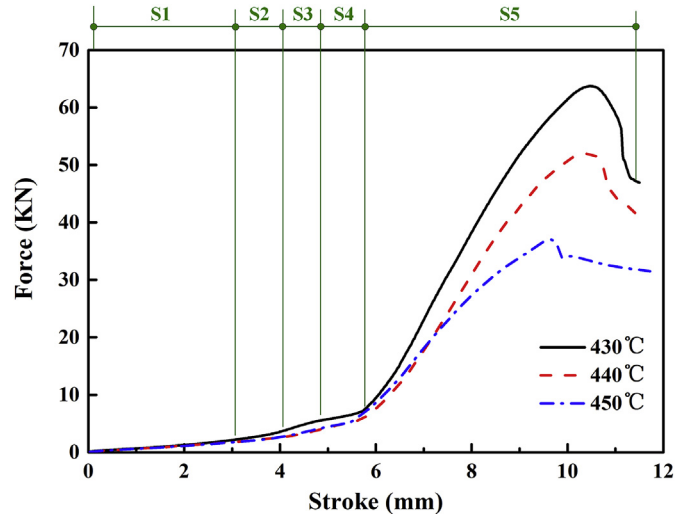


Fig. 4. Force-stroke curves in the extrusion of LM1B and AZ31B samples.

the outlet and the friction between the LM1B and the outlet. The fourth is stage S4 on which the AZ31B sample is extruded into the outlet, and extruded out together with the LM1B sample. The last stage is stage S5 on which only the AZ31B sample is extruded into the outlet, and the temperatures have a significant effect on the force. As the stroke of punch is more than 10 mm, the force begins to reduce due to the reduction of contacting area between the die cavity and sample [24].

Normally, the BMGs thermoplastic deformation mode may exhibit a dramatic change under the prerequisite of temperature rising within SLR. Besides, the BMGs present a linear viscoelastic flow at a low strain rate without a stress overshoot caused by the amorphous viscoelastic structure relaxation during SLR has been reported in the previous literature [6,19]. Therefore, the force-stroke curve shows a limited increase at an extremely low strain rate in this work, implying a typically Newtonian rheological state, as the stages S1, S2 and S4 shown in Fig. 4. In addition, the peak of extrusion force decreases gradually with the increasing of heating temperature.

Fig. 5 exhibits a clear schematic diagram of the whole extrusion process and deformation mechanism. After the die has been heated to a specified temperature, the LM1B BMG plate, AZ31B cylinder and the punch are inserted into the die in order, as shown in Fig. 5 (a). After heated for 2 min to ensure the temperature uniformity, the LM1B BMG plate and AZ31B cylinder are extruded into the outlet of die in order at a slow strain rate, as seen in Fig. 5 (b). Considering the shearing

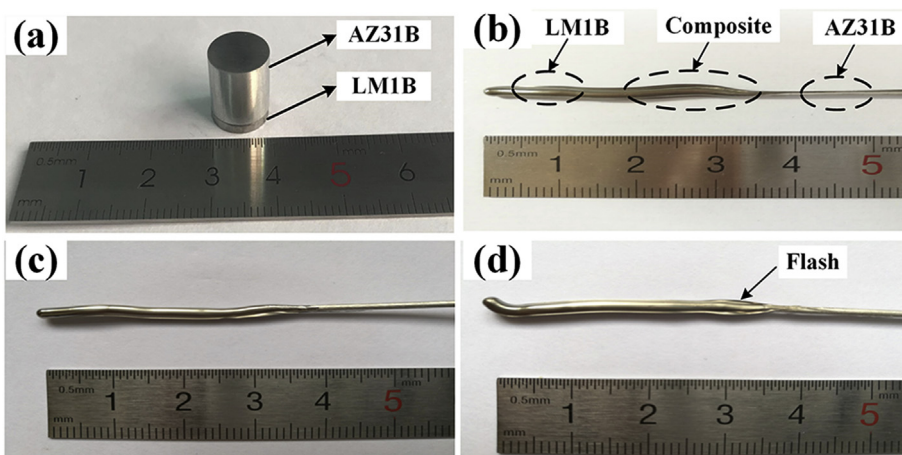


Fig. 3. Samples before and after extrusion, (a) Initial appearance of AZ31B and LM1B samples before extrusion, (b), (c) and (d) Appearance of sample 1, sample 2 and sample 3 after extrusion.

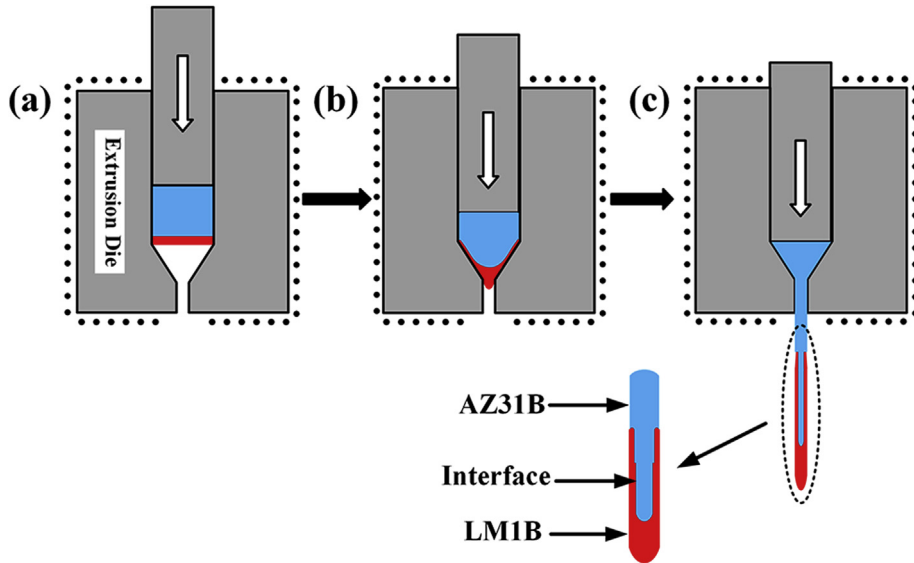


Fig. 5. Schematic diagram of extrusion process, (a) First extrusion step, (b) Second extrusion step, (c) Final extrusion step.

deformations of LM1B BMG and AZ31B, the deformation in the core is significantly more than that of outer in the extrusion process. On the base of considering the strong debonding around interface, the drastic relative motion and friction between the LM1B BMG and AZ31B are highly relevant, as well as the LM1B BMG viscously flows under the pressure. In addition, the severe friction-induced crack damage can be found in close vicinity to the interface and extruded surface [21]. So, the AZ31B is tightly wrapped in the LM1B BMG, and extruded into the outlet of die together with the LM1B BMG. Finally, the AZ31B without the clad of LM1B BMG is extruded into the outlet of die, as shown in Fig. 5 (c).

3.2. Characterization of interface

Fig. 6 presents the OM pictures of the overall appearance in the cross section of the interface. It is shown that the macroscopic feature of three samples seem to be similar in the cross section, magnesium alloy (AZ31B) is fully wrapped by the LM1B BMG. The smooth and continuous appearance in interface implies that excellent bonding between BMG and AZ31B has come true by the hot stacking extrusion. The

smooth and clean interface displays a series of better joint effect when considering of good appearance with a narrow deformation region, such as defect-free, convenient to the later processing treatment, homogeneous deformation of BMG and good compatibility with crystalline alloys. However, the considerable discrepancy of material structure and flow characteristics result in an obvious deformation incompatibility between BMG and AZ31B [22], which can account for the visible bending deformation in the initial bonding part as shown in Fig. 6. Moreover, the interface of initial bonding part seems to be a semicircle for the extruded sample 2, but the initial bonding part of sample 1 looks more like semielliptical, even more sharp for sample 3 caused by the drastic rheological behavior of BMG with a low viscosity at higher temperature. For sample 1, the temperature is lower than sample 2, higher viscosity with a bad thermal-plastic deformability result in a semielliptical initial bonding between LM1B and AZ31B. Thus, it is concluded that the semicircle interface means stable interface state, and corresponds to more satisfactory bonding effect under proper test temperature.

Fig. 7 presents the SEM images of the different regions at the interface shown in Fig. 6. Fig. 7 (a), (e) and (f) are corresponding to the

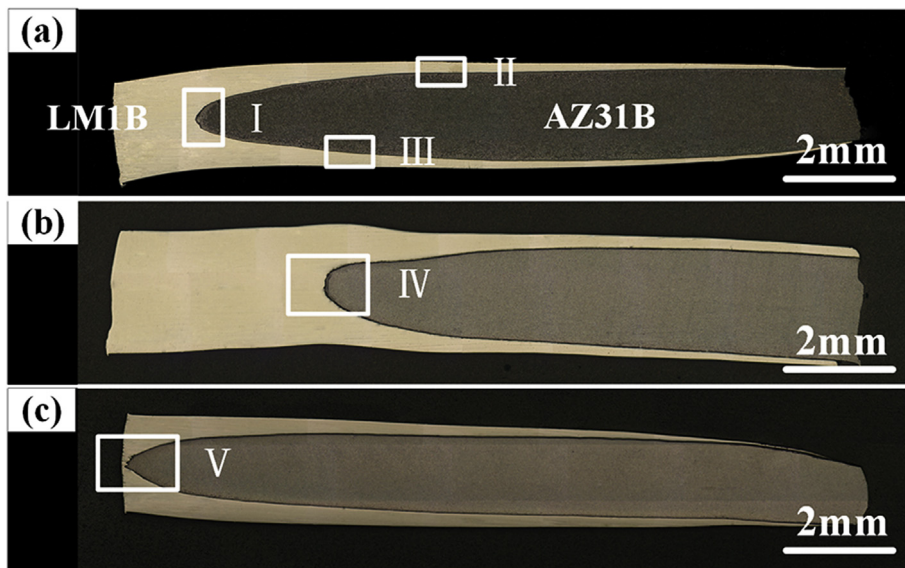


Fig. 6. Pictures of the overall appearance of the cross section of the interface taken by Axiom LabA1 OM, (a) Sample 1, (b) Sample 2, (c) Sample 3.

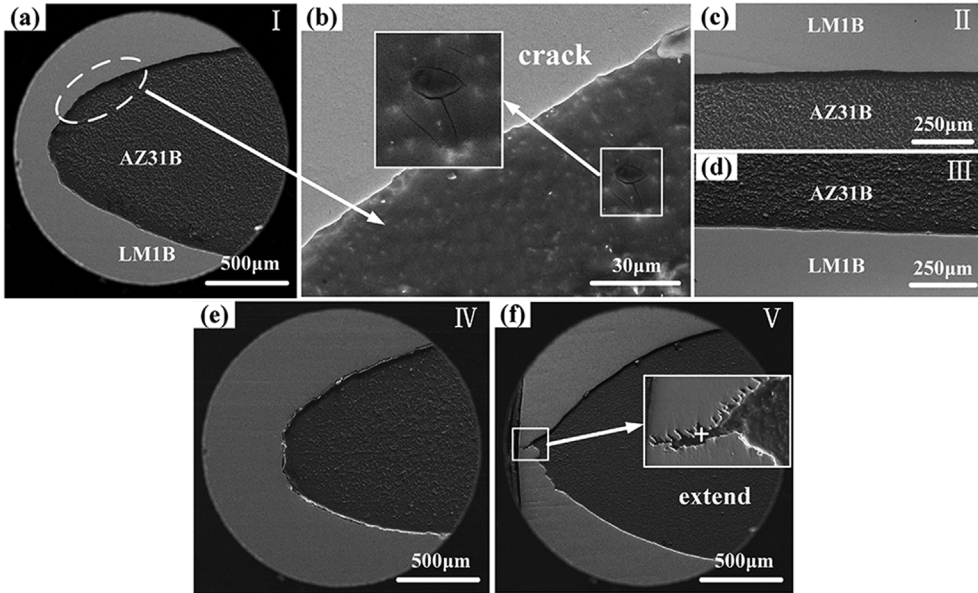


Fig. 7. SEM observation of the LM1B/AZ31B interfaces of extruded samples taken by Nova Nano SEM450. (a) Initial bonding site shown in the region I of Fig. 6; (b) High magnification image of bonding area shown in Fig. 7 (a); (c) The upper bonding area shown in the region II of Fig. 6; (d) The lower bonding area shown in the region III of Fig. 6; (e) Initial bonding site shown in the region IV of Fig. 6; (f) Initial bonding site shown in the region V of Fig. 6.

initial bonding site shown in the regions I, IV and V of Fig. 6, respectively. Fig. 7 (c) and (d) are corresponding to the upper region II and the lower region III in Fig. 6, respectively. It should be emphasized that the interface exhibits clean and smooth appearance, no obvious microcracks, voids, fold deformation, or any other joining defects can be observed between the interface of LM1B and AZ31B. It indicates that the LM1B BMG and AZ31B are joined together by means of fine mechanical bonding, while the weld crack, voids and brittle phase of intermetallic compound appear when the light alloy is joined with BMG by other welding methods [19,22]. It is interesting to note that the shape of initial bonding site shown in Fig. 7 (a), (e) and (f) basically consistent with the counterpart in Fig. 6, but the details can be observed more clearly in Fig. 7 (c) and (d). The local enlarging photograph in Fig. 7 (a) indicated that a truly continuous and smooth interface with a little wave at high magnification, and a microcrack near the interface [21] has also been detected, as shown in Fig. 7 (b). Comparing to the previous work [22], both smooth interface could be generated between the LM1B BMG and light metal alloy (magnesium or aluminum), and some small inhomogeneous wave are found at the vicinity of the boundary indicate typical mechanical bonding. The SEM image shown in Fig. 7 (f) has successfully revealed the microscopic morphology of interface near the initial bonding site in details of sample 3 in the high resolution, which corresponding to the region V in Fig. 6 (c). Moreover, the further amplification of the initial site in Fig. 7 (f) presents an obvious dendritic extend from AZ31B into LM1B BMG, this complex deformation irregularity behavior could be explained by unstable and intensely viscous flow of BMG and exceedingly high compress force [25,26]. SEM and EDX analysis were performed to study the distribution of elements around the dendritic extend region, as shown in Table 2, which demonstrates that a significantly element diffusion from LM1B BMG to AZ31B and a severe oxidation has occurred in the

extrusion process. The EDX result shows that Cu, Ni and Ti elements have an obvious diffusion process from LM1B BMG to AZ31B, especially for Zr in this region, which is caused by a strong interaction and good compatibility between LM1B and AZ31B under the extremely high pressure and temperature condition. Besides, 2 min of pre-heating for each sample to achieve the homogeneous temperature in the die without protective atmosphere is the chief reason for oxidation.

Fig. 8 shows the variation of diameter in the sample 2 shown in Fig. 6 (b). The cross-section of sample shows that the core of sample is AZ31B, and the LM1B BMG is on the outer of sample, as shown in Fig. 8 (a). The sizes of cross-section have been measured precisely by a zeta-20 3D optical profiler, the variations of size percentage are shown in Fig. 8 (b), which is basically in accordance with the cross-section macroscopic image. The deviation of the diameter of the extruded sample should be given a particular attention in this paper, which is plotted in Fig. 8 (c). The curve in Fig. 8 (c) shows that sample 2 has the significant dimension accuracy and stability than the other two samples, which indicates the better superplastic behavior of BMG and compatibility relationship between LM1B and AZ31B can be attained by selecting the extruding temperature at 440 °C.

The amorphous state of LM1B BMG not close to the bonding interface after extrusion has been tested by XRD as illustrated in Fig. 9. The XRD patterns of all the processed samples indicates that the LM1B BMG after the super-plastic deformation basically keeps the amorphous state. However, XRD detection can not completely determine the structure of LM1B BMG in consideration of the limited and tiny crystallized phase is not sensitive to that. So that, the processed BMG state needs further investigation.

For further study on the microscopic structure characteristics in the vicinity of interface in sample 2, TEM observations were also performed and the results are shown in Fig. 10. High resolution image of Fig. 10 (a) exhibits a distinctly boundary between LM1B and AZ31B on the interface, without any voids, cracks or other joining defects. Besides, some irregular blocks embedded in the glass phase side can be seen in Fig. 10 (a), which indicating nanocrystals. In the higher resolution picture of Fig. 10 (b), corresponding to the rectangle I of Fig. 10 (a), a few of regularly arranged atomics could be found among those nanocrystal clusters. There are many reasons account for the appearance of nanocrystals. It has been reported that working at high process temperature close to T_g [1], non-Newtonian deformation at high strain rates [1,4], atomic diffusion [20] and the extremely high pressure [1] are all attributed to the nanocrystallization occurring in the BMG

Table 2

EDX analysis of the interface in SEM (at%).

Elements	Weight%	Atomic%
Zr	37.11	13.34
Cu	5.07	2.61
Ni	5.47	3.05
Ti	4.65	3.18
Mg	26.81	36.14
Al	1.38	1.67
O	19.52	40.00

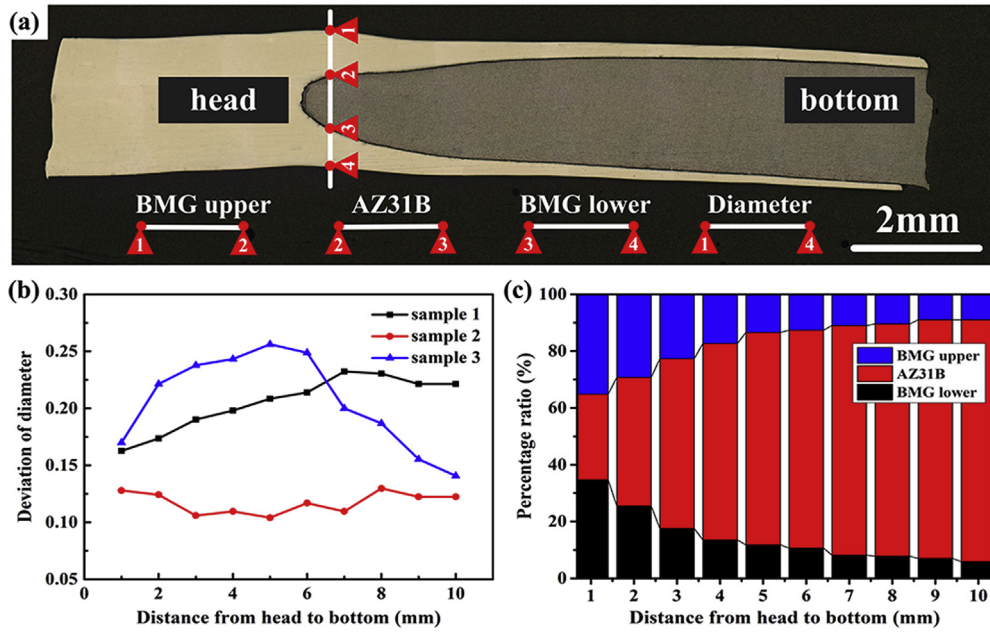


Fig. 8. Cross-section and size variation of sample, (a) Cross-section of sample 2, 1–2 and 3–4 are the size of LM1B, 2–3 is the size of AZ31B, 1–4 is the diameter of sample, (b) Size percentage of LM1B and AZ31B on the cross-section, (c) Variation of diameter for sample 1, sample 2 and sample 3.

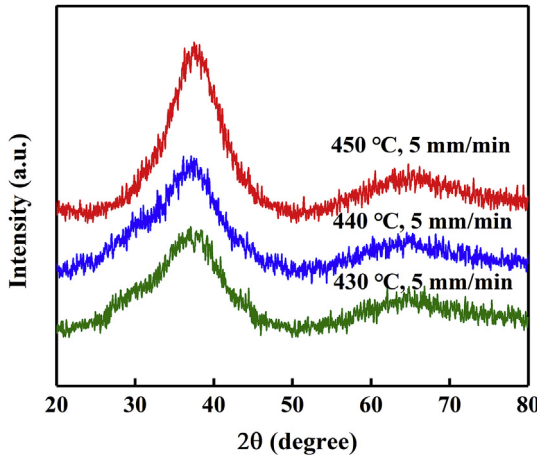


Fig. 9. XRD diffraction patterns of LM1B after extrusion.

matrix during extrusion process. Usually, the nanocrystals appeared, which can improve the mechanical property of metallic glass including hardness and strength [1,2]. It is worth mentioning that the image in Fig. 10 (c), further magnification image of the bonding region (shown in the rectangle II of Fig. 10 (a)), displays a typical transition zone of approximately 20 nm width. Furthermore, three significantly different regions have been detected among the transition zone including the LM1B region, the AZ31B region and the diffusion band area, respectively. The atomic arrangement of AZ31B region shows a better order indicating a typical crystal structure while a disorder and irregular atomic distribution in the LM1B region corresponding to a non-crystal structure. The diffusion band between AZ31B and LM1B displays a complicate material structure, most of the diffusion band shows an amorphous matrix, and part of region in the diffusion band shows a partial crystallization due to the diffusion of elements and working at the high temperature for a long time [1,18,19]. From the HRTEM picture of Fig. 10 (d), an obvious partial crystallization with size less than 10 nm could be easily observed below the boundary line. Given the fact that the nanocrystals are produced in the glass phase and the partial crystallization of BMG appears at the interface, the metallic glass will

not maintain the all-amorphous state after extrusion process.

Moreover, the distribution of elements in the bright-field STEM image (Fig. 11 (c)) has been characterized by STEM EDS analysis, and the five main element maps along the interface are illustrated in Fig. 11(b–f). It can be seen from Fig. 11 (b) that Ti element diffused sufficiently from LM1B into AZ31B in the interface region, and Ni, Cu and Zr elements present a slightly weaker diffusion capacity compared with Ti element in Fig. 11(c–e). For the Mg element, the worst diffusion effect has been observed in Fig. 11 (f). The diffusion of LM1B elements to AZ31B is easier than that of magnesium to LM1B, the atomic diffusion occurs on the interface and narrow diffusion zones are formed usually in the AZ31B site, which is mainly due to the existence of grain boundaries in the crystal alloy and the conditions conducive to the diffusion of atoms such as crystal defects, surface [22,27,28]. However, the atomic arrangement in LM1B is disordered, which is not convenient to the diffusion and propagation of atoms. In addition, the atomic radius of Ti (0.145 nm) and Zr (0.160 nm) elements in the LM1B BMG are similar to the Mg (0.160 nm) element and Cu (0.128 nm) element is slightly different from that of Mg element, and the diffusion ability is also slightly weak. The existence of metallurgical bonding on the interface can promote the diffusion of LM1B elements to AZ31B. The key factor improving the joint quality is attributed to the local crystallization behavior of interface layer, as well as the significant enhancement of the atomic diffusivity after crystallization [29]. Besides, oxide film is the main barrier to element diffusion at the interface, but the oxide film can be weakened through the surface microplastic deformation, and promoting the elements diffuse between the dissimilar materials [5,28]. Furthermore, the diffusion bonding process of LM1B BMG to AZ31B could be divided into two stages: void formation stage in the LM1B side and void shrinkage stage in the AZ31B side [30].

Fig. 12 displays the hardness profile of the LM1B BMG and AZ31B interface. Hardness measurements across the interface layer were carried out at a constant distance of 200 μm between the tested points. The left side illustrates the hardness of LM1B BMG, while the right is the hardness of AZ31B. It is obvious that the LM1B BMG is much harder than AZ31B. As can be found that the hardness of AZ31B and LM1B BMG firstly increases and then decreases to the stable-state as the

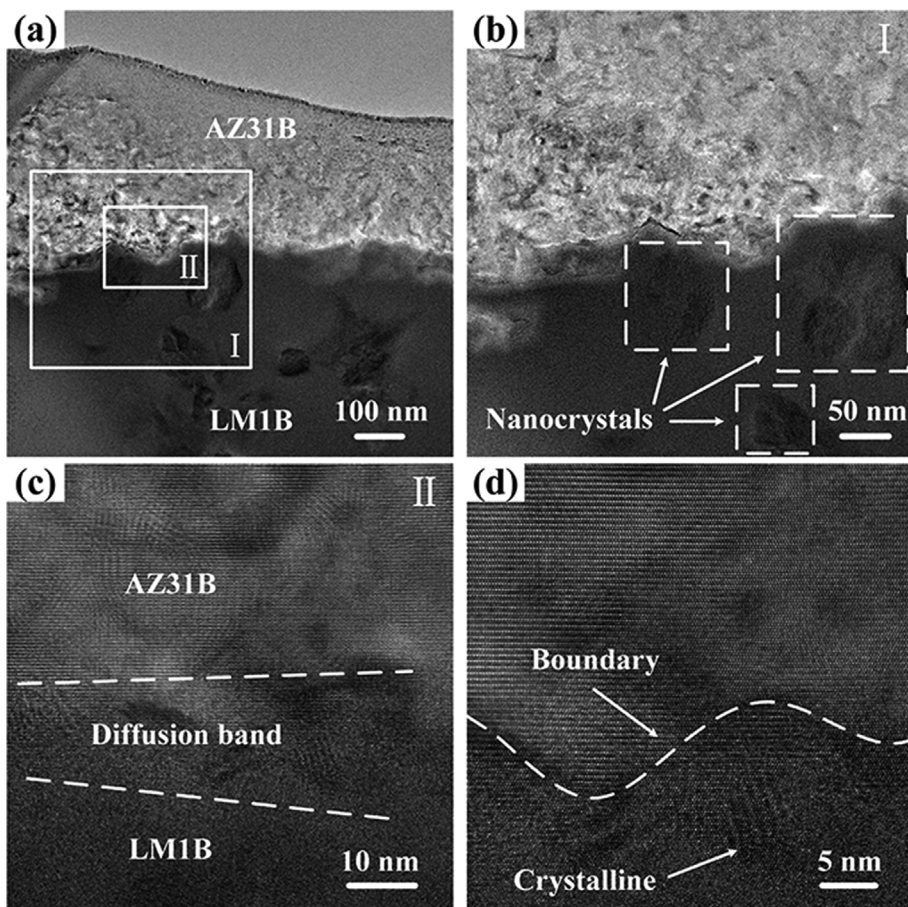


Fig. 10. TEM investigation and elemental mapping results along the interface between BMG and Mg alloy taken by FEI Talos F200X. (a) TEM image along the interface of sample 2; (b) High-resolution image along the interface shown in Fig. 10 (a) I; (c) High-resolution image along the interface shown in Fig. 10 (a) II; (d) High-resolution image of the diffusion band shown in Fig. 10 (c), respectively.

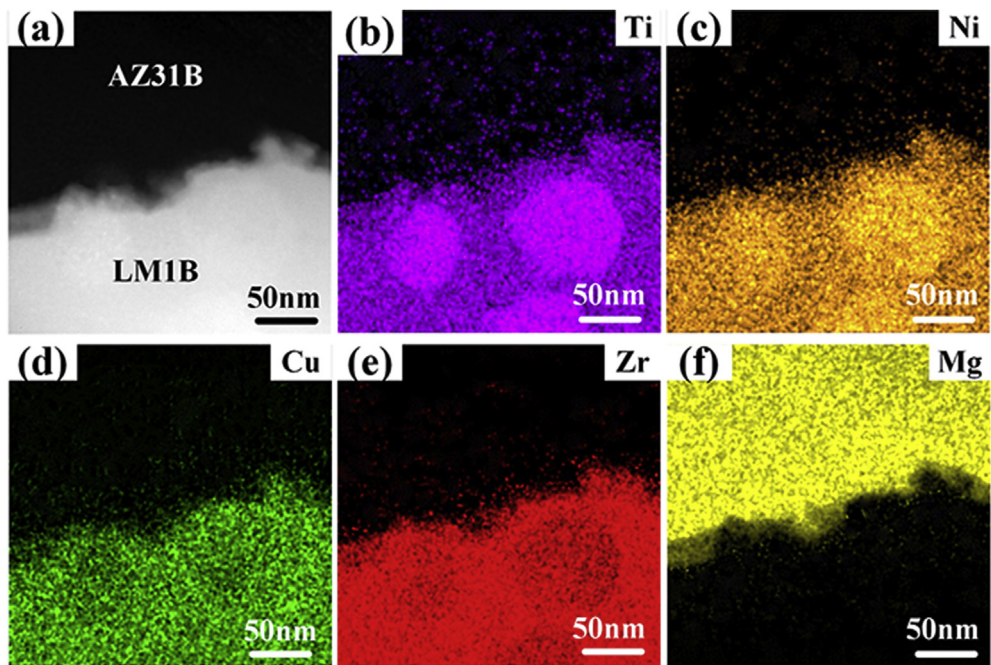


Fig. 11. Elemental mapping results along the interface between BMG and Mg alloy taken by FEI Talos F200X. (a) Bright-field image, (b) Ti, (c) Ni, (d) Cu, (e) Zr and (f) Mg element, respectively.

distance away from the bonding interface. The increasing of the hardness on the interface for both AZ31B and LM1B BMG is closely associated with the phenomena of stress focus, which is induced by the extremely high extrusion force and temperature. Moreover, the

evolution of the hardness is highly relevant to the variation of free volume in the LM1B BMG. It has reported that the hardness of glassy phase increases presumably due to the structural relaxation, which is attributed to the atomic diffusion and rearrangement in the diffusion

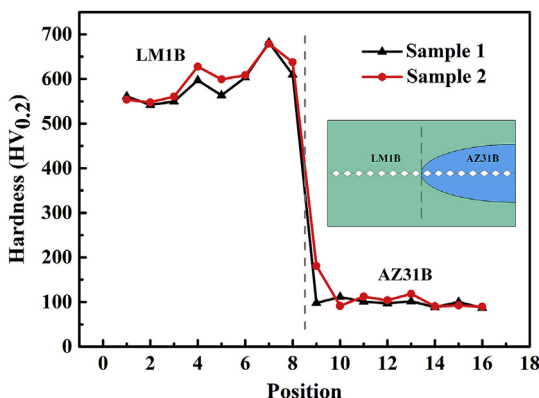


Fig. 12. Vickers hardness in the vicinity of interface.

bonding process [31].

4. Conclusions

LM1B BMG exhibits a good plastic forming ability within the SLR, while the composite structure material of LM1B BMG wrapped on AZ31B alloy can be prepared by stacking hot extrusion method. The extrusion process and the interface characteristics of LM1B/AZ31B composite have been investigated. The results are summarized as follows:

LM1B BMG exhibits a better macroscopic compatibility with magnesium alloy at a relatively low extrusion rate within SLR, especially the flow ability of the BMG increases gradually with the increasing of heating temperature.

The interface between LM1B BMG and AZ31B is well bonded, while the boundary shape is smooth and homogeneous without obvious defects. LM1B BMG and AZ31B are mainly joined together in a mechanical interlocking way, while the remarkable atomic diffusion at the interface indicates the existence of metallurgical bonding between BMG and magnesium. Both the nanocrystals and partial crystallization in the metallic glass indicating that the LM1B no more maintains all-amorphous state after extrusion process.

Acknowledgements

This work was financially supported by the National Natural Science Foundation of China, China (51575324) and Taishan Scholarship of Climbing Plan, China (tspd20161006) and Shandong Province Key Laboratory of Mine Mechanical Engineering, China (2019KLM104).

References

- [1] C.A. Schuh, T.C. Hufnagel, U. Ramamurty, Mechanical behavior of amorphous alloys, *Acta Mater.* 55 (2007) 4067–4109.
- [2] J. Schroers, Processing of bulk metallic glass, *Adv. Mater.* 22 (2010) 1566–1597.
- [3] Y.K. Xu, H. Ma, J. Xu, E. Ma, Mg-based bulk metallic glass composites with plasticity and gigapascal strength, *Acta Mater.* 53 (2005) 1857–1866.
- [4] K.C. Chan, L. Liu, J.F. Wang, Superplastic deformation of Zr55Cu30Al10Ni5 bulk metallic glass in the supercooled liquid region, *J. Non-Cryst. Solids* 353 (2007) 3758–3763.
- [5] W. Chen, Z. Liu, J. Schroers, Joining of bulk metallic glasses in air, *Acta Mater.* 62 (2014) 49–57.
- [6] G.S. Yu, J.G. Lin, W. Li, C.E. Wen, Extrusion properties of a Zr-based bulk metallic glass, *Mater. Lett.* 63 (2009) 1317–1319.
- [7] T. Terajima, K. Nakata, Y. Matsumoto, W. Zhang, H. Kimura, A. Inoue, Brazing of Cu with Pd-based metallic glass filler, *Mater. Sci. Eng. B* 148 (2008) 128–131.
- [8] J. Kim, T. Lee, Brazing method to join a novel Cu54Ni62r22Ti18 bulk metallic glass to carbon steel, *Sci. Technol. Weld. Join.* 22 (8) (2017) 1–4.
- [9] D. Wang, B.L. Xiao, Z.Y. Ma, H.F. Zhang, Friction stir welding of ZrCuAlNi bulk metallic glass Al-Zn-Mg-Cu alloy, *Scripta Mater.* 60 (2009) 112–115.
- [10] H.S. Shin, Y.C. Jung, J.K. Lee, Influence of tool speeds on dissimilar friction stir spot welding characteristics of bulk metallic glass/Mg alloy, *Metall. Mater. Interface* 18 (2012) 685–689.
- [11] H. Zhang, Y.Z. Lu, Y.J. Huang, A. Feng, Z.X. Qin, X. Lu, Joining of Zr₅₁Ti₅Ni₁₀Cu₂₅Al₉ BMG to aluminum alloy by friction stir welding, *Vacuum* 120 (2015) 47–49.
- [12] N.H. Tariq, M. Shakil, B.A. Hasan, J.I. Akhter, M.A. Haq, N.A. Awan, Electron beam brazing of Zr₆₂Al₁₃Ni₇Cu₁₈ bulk metallic glass with Ti metal, *Vacuum* 101 (2014) 98–101.
- [13] G. Wang, Y. Huang, W. Cao, Z. Huang, M. Huttula, Y. Su, C. Tan, Microstructure and crystallization mechanism of Ti-based bulk metallic glass by electron beam welding, *J. Manuf. Process.* 32 (2018) 93–99.
- [14] N. Li, J. Zhang, W. Xing, D. Ouyang, L. Liu, 3D printing of Fe-based bulk metallic glass composites with combined high strength and fracture toughness, *Mater. Des.* 143 (2018) 285–296.
- [15] W. Pilarczyk, The investigation of the structure of bulk metallic glasses before and after laser welding, *Cryst. Res. Technol.* 50 (2015) 700–704.
- [16] D.Z. Wang, N. Li, L. Liu, Magnetic pulse welding of a Zr-based bulk metallic glass with aluminum plate, *Intermetallics* 93 (2018) 180–185.
- [17] X.K. Fan, L. Chen, G.J. Chen, G.Q. Zhao, C.S. Zhang, Joining of 1060/6063 aluminum alloys based on port hole die extrusion process, *J. Mater. Process. Technol.* 250 (2017) 65–72.
- [18] K.S. Lee, H.J. Jun, Y.S. Lee, Fabrication of bimetallic rods consist of a Zr-based bulk metallic glass and a crystalline copper by co-extrusion, *Intermetallics* 18 (2010) 1958–1963.
- [19] K.S. Lee, S.H. Kang, Y.S. Lee, Synthesis of Zr-based bulk metallic glass-crystalline aluminum alloy composite by co-extrusion, *Mater. Lett.* 64 (2010) 129–132.
- [20] Y. Liu, J.J. Blandin, G. Kapelski, M. Suéry, X.J. Yang, Interface characterization and mechanical properties of BMG/Cu composites prepared by coextrusion, *Intermetallics* 30 (2012) 57–64.
- [21] S. Gravier, J.J. Blandin, M. Suéry, Mechanical properties of a co-extruded Metallic Glass/Alloy (MeGA) rod-Effect of the metallic glass volume fraction, *Mater. Sci. Eng. A* 527 (2010) 4197–4201.
- [22] R. Jiang, H.P. Li, Z.C. Li, L.F. He, Fabrication of Zr-based bulk metallic glass/aluminum alloy multi-materials by stacking extrusion, *Vacuum* 149 (2018) 79–82.
- [23] Z.F. Yao, J.C. Qiao, J.M. Pelletier, Y. Yao, High temperature deformation behaviors of the Zr_{63.36}Cu_{14.52}Ni_{10.12}Al₁₂ bulk metallic glass, *J. Mater. Sci.* 51 (2016) 4079–4087.
- [24] F.F. Dong, J. Zhou, Z.W. Liu, G. Wang, L.X. Li, Simulation for AM80 magnesium alloy sheet hot extrusion, *Mater. Mech. Eng.* 36 (10) (2012) 77–85.
- [25] A. Volland, J. Ragan, Y. Liu, S. Gravier, M. Suéry, J.J. Blandin, Design of multi materials combining crystalline and amorphous metallic alloys, *J. Alloy. Comp.* 536 (2012) S143–S147.
- [26] X. Wu, J.J. Li, Z.Z. Zheng, J.Y. Li, The effect of forming speed on the formability of a Zr-based bulk metallic glass, *Adv. Mater. Res.* 1088 (2015) 265–271.
- [27] C. Wen, T.L. Shi, B. Chen, Z.J. Zhu, Y. Peng, Guanglan Liao, Diffusion bonding of Zr₅₅Cu₃₀Ni₅Al₁₀bulk metallic glass to Cu with Al as transition layer, *Mater. Des.* 83 (2015) 320–326.
- [28] H.C. Kou, H. Guan, J. Wang, B. Tang, J.S. Li, Diffusion bonding between Zr-based metallic glass and copper, *Rare Metal Mater. Eng.* 45 (2016) 42–45.
- [29] J. Cao, H.Y. Chen, X.G. Song, J.K. Liu, J.C. Feng, Effects of Ar ion irradiation on the diffusion bonding joints of Zr₅₅Cu₃₀Ni₅Al₁₀ bulk metallic glass to aluminum alloy, *J. Non-Cryst. Sol.* 364 (2013) 53–56.
- [30] H.Y. Chen, J. Cao, J.K. Liu, X.G. Song, J.C. Feng, Contributions of atomic diffusion and plastic deformation to the diffusion bonding of metallic glass to crystalline aluminum alloy, *Comput. Mater. Sci.* 71 (2013) 179–183.
- [31] H.S. Chou, J. Huang, L.W. Chang, T.G. Nieh, Structural relaxation and nanoindentation response in Zr–Cu–Ti amorphous thin films, *Appl. Phys. Lett.* 93 (2008) 191901–191901-3.